Galactic Mergers NGC 5394 & NGC 5395.

Máximo Rodríguez Herrero
Tutor: Gwendolyn Meeus

This observational study of the NGC 5394 and 5395 merging system, conducted with the $2.2m$ telescope of the Calar Alto Observatory (Spain), focused on the system's structure and stellar population. The study confirmed that NGC 5395 is a spiral galaxy, while NGC 5394 is hypothesized to be a barred spiral galaxy, pending further research. The presence of high population I stars and the distortion of the spiral arms in the intermediate region suggest that the galaxies are beginning to merge. `https://github.com/MaximoRdz/GALAXY-MERGERS-TFG`

I. OBSERVING PROGRAMME

The system is formed by two spiral galaxies **NGC-5395** (α: 13^h 58^m 38.3^s; δ: $+37^o25'32"$) and **NGC-5394** (α: 13^h 58^m 33.8^s; δ $+37^o27'18"$) using the right ascension, α, and the declination, δ, coordinates. This system was characterized using the Cafos $2.2m$ telescope and the Johnson photometric filters (B, R and V bands). The observation combined short exposures (one exposure of 60 seconds) and long exposures (one exposure of 900 seconds) for each band mention above. In order to study the specific composition of the galaxy, one extra exposure of 1200 seconds was taken using the H_α narrow band.

II. STRUCTURE CHARACTERIZATION

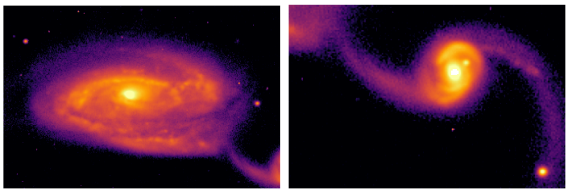

FIG. 1. NGC 5395 (Left) and NGC 5394 (Right)

The spiral galaxy NGC 5395 is the larger of the two, its morphology is perfectly spiral except a small distortion of the lower arm due to the interaction with NGC 5394 (the gravitational pull is dragging both together). NGC 5394 has also a spiral structure although the observation suggest the presence of a bar in the bulge of the galaxy making it a barred spiral galaxy (according to Hubble's sequence).
Since neither of them have been really distorted it can be interpreted as one of the early stages of the merging.

III. STELLAR COMPOSITION

The stellar population of the galaxy can be divided into two groups according to their color index, $B-V$ (with Vega as a zero point). The lower the color index is the bluer, the emissions are and, conversely, the larger it is, the redder. The criteria use to define the division of population is based on a simple approximation to the MK spectral classification system [1], considering O, B, A, F and G types as population I ($B-V<0.8$)and M and K types population II stars ($B-V>0.8$)

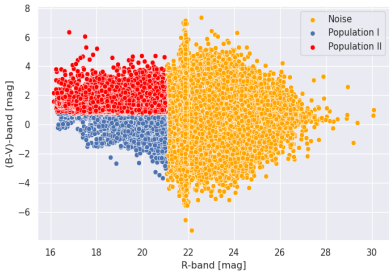

FIG. 2. Color index. The maximum resolution achieved is around magnitude 21 so no data faintest than that is considered.

1. *Population I*

Formed by young metal-rich stars and more commonly found in the spiral arms. As predicted by the theory the young stars are clearly located in the outer regions of both galaxies, figure 3. Close to the union of the spiral

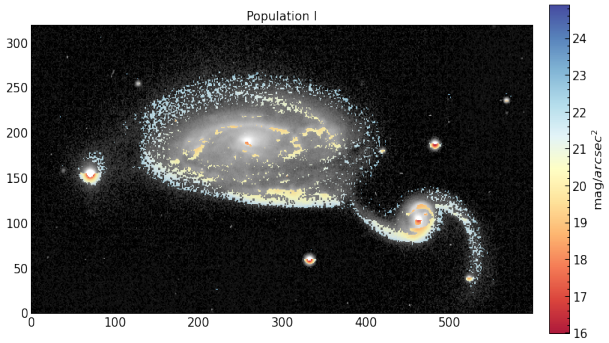

FIG. 3. Population I is observed to be distributed in the spiral arms of both galaxies.

arms of both galaxies (figure 3) the presence of population I stars intensifies (in contrast to the regions in the

extremes) suggesting a highly star-forming region. This could be due to the frictional interaction of the gas between the galaxies (capable of forming new stars).

2. *Population II*

Formed by metal-poor stars. The observation perfectly agrees with the expected high abundance of old, red stars in the bulges of both galaxies, figure 4.

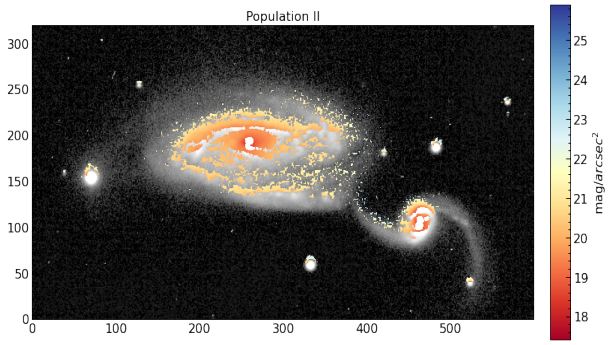

FIG. 4. The spatial distribution of Population II stars is predominantly concentrated in the inner regions of the galaxies.

A. RGB Image

Combining the images in the three bands (the three primary colors), see code [5], the pixels can be colored resulting in the following image. The reddish color is caused by the dominant red presence. One reasonable explanation is the attenuation of shorter wavelengths (B and V) caused by dust.

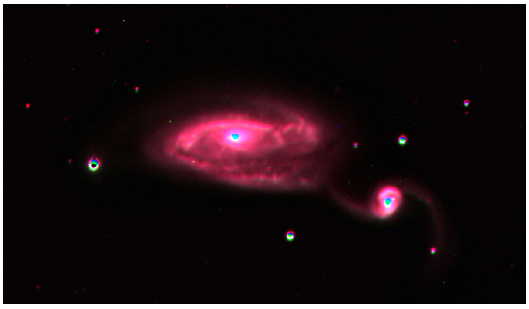

FIG. 5. RGB image of the merging system. Proper alignment of the images would be required to conduct further and better research.

IV. IMAGE REDUCTION

The number store in the images provided by Cafos is called Analog Digital Unit (ADU) or count, generated via the photoelectric effect. These raw images are referred to as R_{raw}. This image is susceptible to several sources of noise. Image reduction is the process of removing all of these.

A. Bias

To ensure there are no negative counts in the read out, a voltage offset is manually applied to the CCD. The master bias, M_{bias}, was computed taking the median of the 10 separate bias images (shutter closed and zero exposure time).

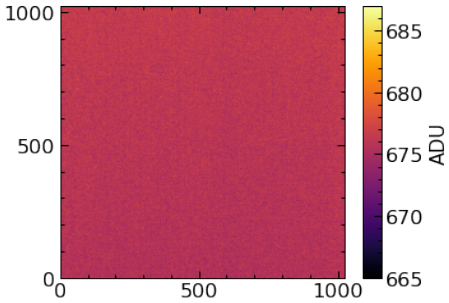

FIG. 6. Master Bias frame.

B. Flats

Used to correct any non-uniformity of the CCD response to light (damaged pixels, dust on the detector, vignetting, etc.). In this observation, dome flats were taken for the Johnson filters and sky flats for H_α.

$$F_i = \frac{R_{raw} - M_{bias}}{< F_i >}$$

where $< F_i >$ represents the median of the ith flat image. Finally, for each filter, $M_{flats} =< F_{i=1,...,N} >$ with N the total number of exposures of a filter.

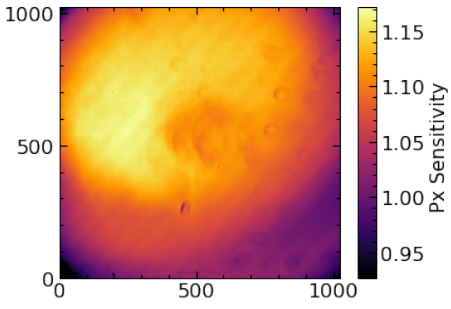

FIG. 7. Master Flat example, Johnson R.

C. Bias and Flats Reduction

Reducing bias noise and correcting for imaging artifacts as follows, $R_{obs} = \frac{R_{raw} - M_{bias}}{M_{flats} \cdot t_{exp}}$ with t_{exp} the exposure time of the raw image.

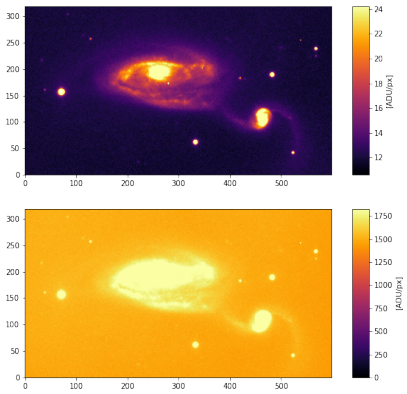

FIG. 8. Image reduced of bias and flats (top) compared to the raw exposure (bottom).

D. Sky Subtraction

Now that every count is due to photons reaching the CCD, it is necessary to remove the contribution of the sky background (moonlight [13], light pollution, etc.). The method involves subtracting the image of the median number of counts of the region outside the rectangle that contains both galaxies (see SkyInteractive [5])

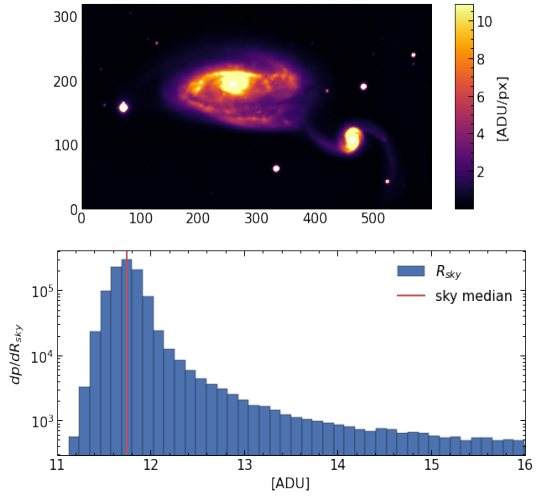

FIG. 9. Sky subtracted image (top). Count distribution of the raw exposure (bottom).

E. Flux Calibration

First, the total counts coming from each calibration star, figure 14, is computed (Astropy's calibration module [2]). The counts of every star, i, have a related magnitude, $m^i_{counts} = -2.5 \log N^i_{counts}$.

Thus, the extinction constant results from the comparison with the tabulated values [3] ,

$$C^i_{ext} = m^i_{counts} - m^i_{tab}$$

Finally, and for every filter, f, the extinction constant is determined as, $C^f_{ext} =< C^{i=1,\dots,N}_{ext} >$ with N the number of calibration stars. The science image in magnitudes per pixel is then computed as,

$$m^f_{obs} = -2.5 \log R^f_{obs} - C^f_{ext}$$

The change to arcsec units depends on the CAFOS $2.2m$ pixel aperture ($scale = 0.53 \cdot \frac{arcsec}{px}$). Until now, $R^f_{obs}[mag/px^2] = -2.5 \log(R^f_{obs}[counts/s/px^2])$. Therefore, the corresponding image can be easily computed as,

$$\begin{aligned} R^f_{obs}[mag/arcsec^2] &= -2.5 \log(\frac{R^f_{obs}[counts/s/px^2]}{scale^2}) \\ &= R^f_{obs}[mag/px^2] + 2.5 \cdot \log([scale^2]) \end{aligned}$$

Lastly, it is useful to work with the units $erg/s/cm^2$, so using the zero points with respect to Vega [4] results in,

$$R^f_{obs}[erg/s/cm^2] = F^f_0 \cdot 10^{-0.4 \cdot R^f_{obs}[mag/arcsec^2]}$$

F. Reduced Images

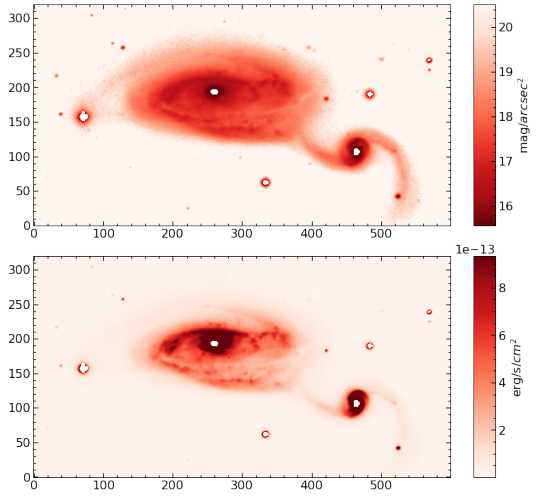

FIG. 10. Johnson R final reduced image both in $mag/arcsec^2$ and $erg/s/cm^2$

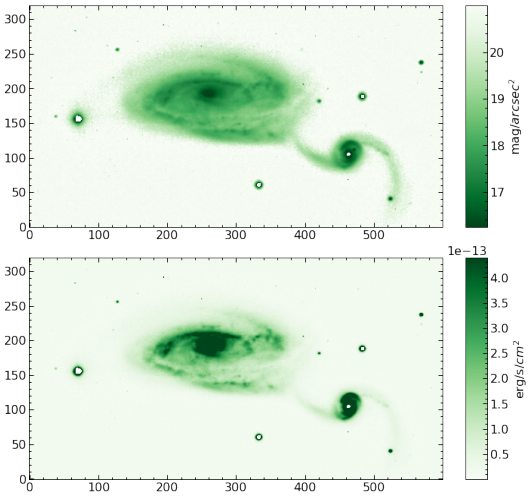

FIG. 11. Johnson V final reduced image both in $mag/arcsec^2$ and $erg/s/cm^2$

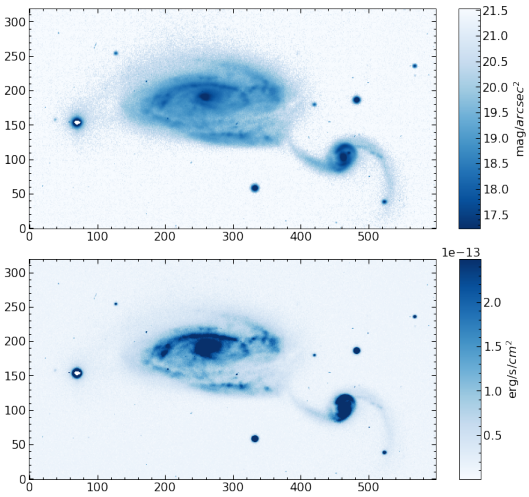

FIG. 12. Johnson B final reduced image both in $mag/arcsec^2$ and $erg/s/cm^2$

FIGURES

Object Visibility

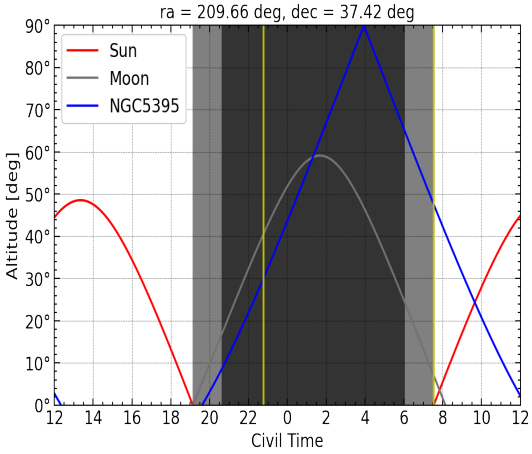

FIG. 13. The best time to observe the galaxies with minimal sky background noise and lowest air-mass is during the time of maximum angular distance between them and the moon, which occurs between 1am and 6am. To ensure that the object is observable by the telescope, the time interval is delimited by vertical yellow lines, which indicate when the object is 30^{o} above the horizon.

Calibration Stars

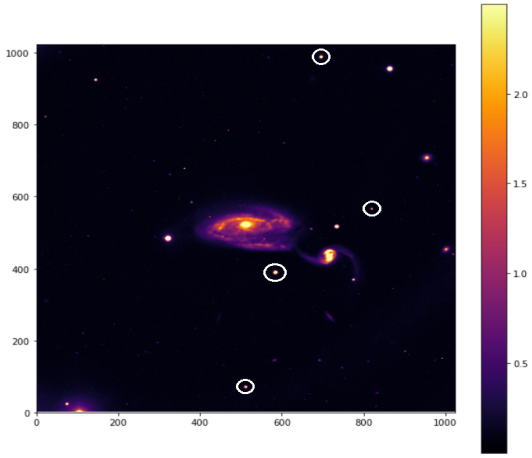

FIG. 14. Calibration stars used. Selection method described in CalibrationStars class (python code [5]).

From top to bottom:

- SDSS ID: 1237662225149722764
- SDSS ID: 1237662225149722679
- SDSS ID: 1237662225149722675
- SDSS ID: 1237662225149722629

[1] Zombeck, Martin V. (1990). "Calibration of MK spectral types". Handbook of Space Astronomy and Astrophysics (2nd ed.). Cambridge University Press. p. 105. ISBN 0-521-34787-4.
[2] https://photutils.readthedocs.io/en/stable/aperture.html
[3] https://skyserver.sdss.org/dr18/
[4] http://svo2.cab.inta-csic.es/theory/fps/index.php?mode=browse&gname=CAHA&gname2=CAHA&asttype=
[5] https://github.com/MaximoRdz/GALAXY-MERGERS-TFG